ISSN 1995-0780, Nanotechnologies in Russia, 2015, Vol. 10, Nos. 5–6, pp. 362–369. © Pleiades Publishing, Ltd., 2015.
Original Russian Text © A.G. Belozerov, N.S. Karasev, N.L. Ovchinnikov, M.F. Butman, 2015, published in Rossiiskie Nanotekhnologii, 2015, Vol. 10, Nos. 5–6.

Formation of Layered Columnar Structure of Montmorillonite by Successive Intercalation of Polyvinyl Alcohol and Aluminum Polyhydroxocomplexes

A. G. Belozerov, N. S. Karasev, N. L. Ovchinnikov, and M. F. Butman

Ivanovo State University of Chemistry and Technology, pr. Sheremetevskii 7, Ivanovo, 153000 Russia

e-mail: belozerovartem@rambler.ru

Received November 17, 2014; accepted for publication February 12, 2015

Abstract—We proposed a new method for the formation of a layered columnar structure of carbon-containing montmorillonite by the successive intercalation of polyvinyl alcohol and aluminum polyhydroxocomplexes $[Al_{13}O_4(OH)_{24}(H_2O)_{12}]^{7+}$. Polyvinyl alcohol was shown to play an important role, serving as an efficient delaminating agent at the step of polycation intercalation into the interlayer space of montmorillonite and, at the step of pillar formation, to favor the formation of thermally stable layered-columnar structure. It was shown that, irrespective of the amount of polymeric intercalate (at its level of 3–20 wt %), the basal distance in the hybrid materials obtained upon a calcination temperature of 450°C is fixed at a value of d_{001} = 1.85 nm and greater than that of the conventional Al_2O_3-pillar montmorrilonite by the thickness of graphene monolayer. The textural characteristics of this layered columnar system can be controlled by the amount of polymer added and by the calcination temperature.

DOI: 10.1134/S1995078015030039

INTRODUCTION

In recent years, pillar (or columnar) materials based on natural layered aluminosilicates (LAS) have attracted intense interest [1]. In an effort to achieve structural and chemical diversities of pillars (which are nanosized clusters of metal oxides) in order to improve their functionalities and increase size and thermal stability, researchers have obtained materials possessing unique textural (high surface area and regular distribution of mesopores) and catalytic (presence of active sites on pillars) properties [2].

The main step in the synthesis of pillar materials is the intercalation of large metal polyhydroxocomplexes into the interlayer space of LAS and the most common intercalating agents are aluminum polycations $[Al_{13}O_4(OH)_{24}(H_2O)_{12}]^{7+}$, the so-called Keggin ions (commonly designated as Al_{13}). For example, their introduction into the interlayer space of montmorillonite (MM) results in an increase in the basal distance d_{001} up to 0.6 nm [3]. This fact has been used in the preparation of polymer-phyllosilicate nanocomposites. In particular, the preliminary delamination of the MM silicate layers with the Al_{13} ions was found to favor its efficient exfoliation in the polyvinyl alcohol (PVA) matrix [4], which, in turn, improves many of the performance characteristics of the initial polymer. On the other hand, the synergistic effect of two different intercalates can be also useful when preparing pillar LAS, namely, the preliminary delamination of the MM silicate layers due to the addition of a water-soluble polymer in small amounts can be supposed to facilitate the intercalation of the Al_{13} polycations [5]. In addition, while realizing this idea, it is interesting to trace probable changes in the properties of pillar carbon-containing MM compared to that prepared by the conventional procedure. The thermal degradation of polymer during pillar formation can play an important role, supposing that the decomposition products formed as radicals can have an effect on pillar structuring due to the grafting and chemical cross-linking processes [6].

The aim of the present work is to obtain mesoporous hybrid materials with carbon-enriched layered columnar structures from the starting aqueous suspensions of montmorillonite and polyvinyl alcohol supplemented with the Al_{13} polycations.

EXPERIMENTAL MATERIALS

MM was isolated from the natural bentonite of Dash-Salakhlinsk field deposits [7] by sedimentation: clay (20 g) was mixed with distilled water (1 L). After 24 h standing, the upper part of suspension was centrifuged. The isolated MM fraction was dried at 80°C. MM was enriched with the Na^+ ions by addition of 1 M NaCl to a suspension (10 g of MM per 1 L of solution) with vigorous stirring on a heating magnetic stir-

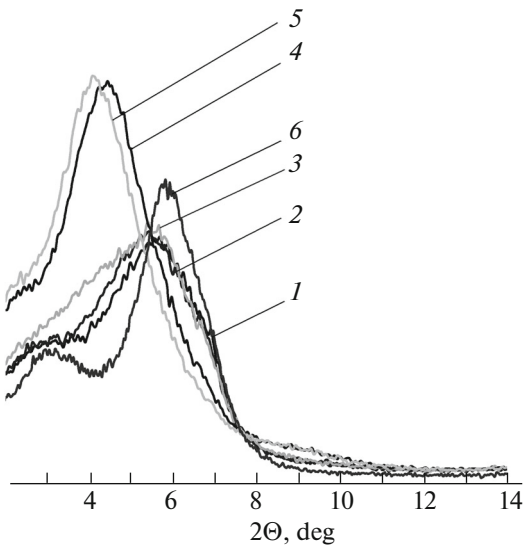

Fig. 1. Small-angle X-ray diffraction patterns for the *x*PVA-MM samples: (*1*) 3PVA-MM, (*2*) 5PVA-MM, (*3*) 10PVA-MM, (*4*) 15PVA-MM, (*5*) 20PVA-MM, and (*6*) initial MM.

rer at 80°C for 2 h. The resulting suspension was washed off from Cl^- ions using distilled water until there was a negative reaction to $AgNO_3$, centrifuged, and dried at 100°C.

PVA (AcrosOrganics, 88% degree of hydrolysis, and molecular weight of 88000) was used as the water-soluble polymer.

PROCEDURE FOR THE PREPARATION OF PILLAR MM

Preliminary polymeric delamination of silicate layers was carried out by the addition of PVA to a 1% suspension of MM preheated to 60°C (1 g of MM per 100 mL of H_2O) based on 3, 5, 10, 15, and 20 wt % of PVA with regard to dry MM. To prepare PVA-MM composites, these suspensions were dried at 60°C. The dried samples are designated hereinafter as *x*PVA-MM ($x = 3$, 5, 10, 15, and 20).

An intercalating solution containing Al_{13} was prepared by the room-temperature hydrolysis of a 0.2 M $AlCl_3 \cdot 6H_2O$ with 0.2 M NaOH at a molar ratio of $[OH^-]/[Al^{3+}] = 2.4$ at pH = 4.3–4.7. The solution was then subjected to ageing for 24 h at 60°C to result in the formation of Al_{13} [8, 9]. The intercalation of the Al_{13}-polycation-delaminated MM was performed by ion exchange in a suspension of MM with preadded PVA: the intercalating solution (50 mL) was added dropwise to the suspension (100 mL) with vigorous stirring on a magnetic stirrer for 2 h at 60°C. After 24 h coagulation at room temperature, the suspension was washed off from Cl^- ions, centrifuged, and dried in a drying cabinet at 60°C. The intercalated samples are referred hereinafter to as Al_{13}-*x*PVA-MM.

Pillar materials were obtained by calcination of the intercalated Al_{13}-*x*PVA-MM samples at 300, 450, and 600°C. They are referred hereinafter to as PMM(*x*PVA).

METHODS OF ANALYSIS

The basal distances d_{001} of the samples were measured by small-angle diffractometry on an upgraded DRON-3 X-ray diffractometer in the CuK_α radiation. The IR spectra of materials synthesized were recorded on an Avatar 360 FT-IRESP Fourier-transform spectrometer. Raman spectra were obtained using a RenishawinViaReflex spectrometer equipped with a CCD detector and helium-neon laser (633 nm). The sorption characteristics and transverse pore size of the samples were determined by low-temperature nitrogen adsorption–desorption on an ASAP 2020 analyzer (Micromeritics).

RESULTS AND DISCUSSION

The small-angle X-ray diffraction patterns of the PVA-MM composites dried at 60°C are shown in Fig. 1 and their basal distances d_{001} are given in Table 1.

Table 1. Basal distances d_{001} (nm) for MM, Al_{13}-MM, the *x*PVA-MM and Al_{13}-*x*PVA-MM composites, and the PMM and PMM(*x*PVA) pillar materials

T, °C	d_{001}, nm					
	MM	3PVA-MM	5PVA-MM	10PVA-MM	15PVA-MM	20PVA-MM
60	1.47	1.62	1.60	1.63	1.94	2.00
	Al_{13}-MM	Al_{13}-3PVA-MM	Al_{13}-5PVA-MM	Al_{13}-10PVA-MM	Al_{13}-15PVA-MM	Al_{13}-20PVA-MM
60	1.64	1.70	1.81	1.92	2.01	2.02
	PMM	PMM(3PVA)	PMM(5PVA)	PMM(10PVA)	PMM(15PVA)	PMM(20PVA)
300	1.63	1.69	1.73	1.76	1.85	1.85
450	–	1.85	1.85	1.85	1.85	1.85
600	–	1.85	1.85	1.85	1.85	1.85

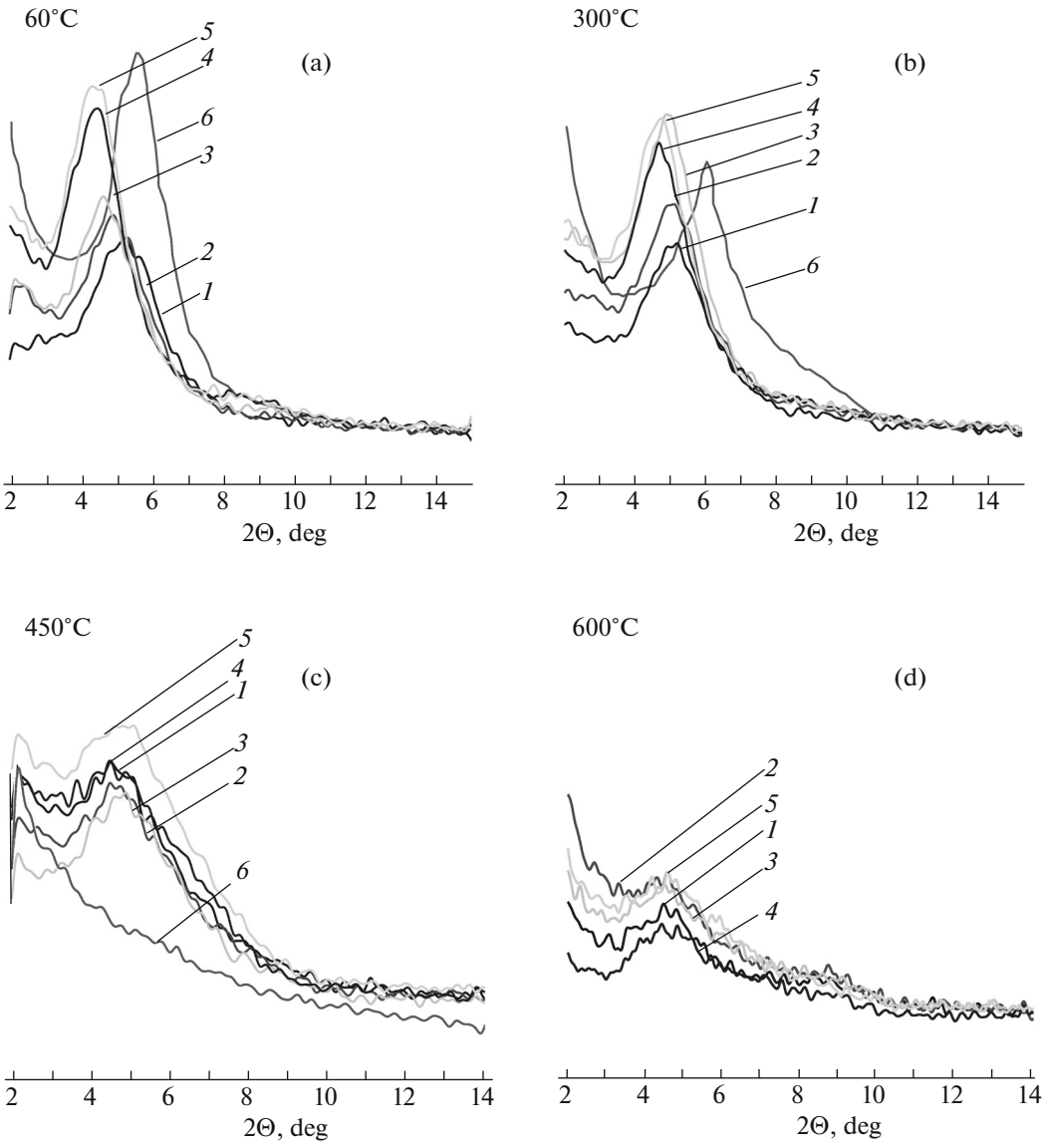

Fig. 2. Small-angle X-ray diffraction patterns for the Al_{13}-*x*PVA-MM samples (a): (*1*) Al_{13}-3PVA-MM, (*2*) Al_{13}-5PVA-MM, (*3*) Al_{13}-10PVA-MM, (*4*) Al_{13}-15PVA-MM, (*5*) Al_{13}-20PVA-MM, and (*6*) Al_{13}-MM, and those for the PMM(*x*PVA) samples (b–d): (*1*) PMM(3PVA), (*2*) PMM(5PVA), (*3*) PMM(10PVA), (*4*) PMM(15PVA), (*5*) PMM(20PVA), and (*6*) PMM.

The d_{001} value in composites having different content of PVA (from 1.62 to 2.0 nm) was found to be greater than that in the starting MM, which suggests the successful intercalation of the PVA molecules into the interlayer space of MM. However, the subsequent calcination of the samples at 300°C causes a decrease in the basal distance down to a value close to the starting MM as a result of PVA burning in the MM interlayer space.

Figure 2 shows the small-angle X-ray diffraction patterns for the samples of Al_{13}-*x*PVA-MM (Fig. 2a) and PMM(*x*PVA) (Figs. 2a–2c) and the corresponding basal distances are given in Table 1.

It is seen from Table 1 that the intercalation of the Al_{13} polycations into MM in the presence of PVA allows one to increase the basal distances compared to Al_{13}-MM obtained by the conventional method. The d_{001} value in Al_{13}-*x*PVA-MM increases slightly compared to *x*PVA-MM at low PVA contents (3, 5, and 10 wt %) and remains virtually unchanged at high PVA contents (15 and 20 wt %). This is likely due to the fact that the increase in the PVA content in the interlayer space to certain level results in ion exchange intensification due to the delaminating effect, which, on the other hand, is restricted by achieving the negative charge balance of the silicate layers.

Table 2. Textural characteristics of the samples

Sample	T, °C	S_{BET}, m^2/g	V_{mp}, cm^3/g	V_{msp}, cm^3/g	ΣV_{pore}, cm^3/g	D_{av}, nm
MM	60	98	0.015	0.196	0.21	8.62
PMM	300	131	0.038	0.147	0.18	5.53
PMM(3PVA)		112	0.032	0.141	0.17	5.95
PMM(5PVA)		109	0.021	0.154	0.18	6.55
PMM(10PVA)		73	0.004	0.135	0.15	8.02
PMM(15PVA)		100	0.007	0.156	0.17	6.94
PMM(20PVA)		92	0.006	0.142	0.16	6.88
PMM(3PVA)	450	103	0.025	0.130	0.15	6.00
PMM(5PVA)		102	0.021	0.136	0.16	6.22
PMM(10PVA)		131	0.029	0.153	0.18	5.56
PMM(15PVA)		108	0.023	0.127	0.15	5.57
PMM(20PVA)		90	0.013	0.114	0.13	5.80
PMM(3PVA)	600	49	0.002	0.121	0.13	10.68
PMM(5PVA)		60	0.008	0.134	0.15	9.77
PMM(10PVA)		81	0.012	0.142	0.16	7.79
PMM(15PVA)		99	0.019	0.156	0.18	7.19
PMM(20PVA)		121	0.027	0.166	0.19	6.36

Calcination of Al_{13}-MM and Al_{13}-xPVA-MM at 300°C, when the pillar system is already partially formed, according to expectations, resulted in a decrease in d_{001} (Table 2). However, there remained a tendency for the increase in d_{001} with an increase in the PVA content in the starting composites.

Most importantly, the basal distances in all pillar samples became equal after calcination at 450°C, although there was some decrease in the intensity of small-angle reflex and its broadening. No less intriguing was the fact that the same value of $d_{001} = 1.85$ nm remained also after the calcination at 600°C, given the fact that, in the conventionally prepared PMM samples, the full collapse of pillar structure occurs even at a calcination temperature of 450°C. The latter conclusion follows from Fig. 2c, where the small-angle basal reflex (001) disappears almost completely.

The carbon layers formed within the interlayer space of MM are known to act as the protector of layered structure at high temperatures (⩾450°C) [10]. It is extremely interesting to note that the difference between the d_{001} values in PMM and PMM(xPVA) is 0.32 nm, which, taking into account the measurement error of the basal distance d_{001} (±0.01 nm), corresponds to the grapheme monolayer thickness of 0.33 nm [11]. The carbonation of PVA to form graphene is a real process, since PVA undergoes thermal destruction to form a large number of C=C bonds [12]. Taking into account the data of [10], this result can reflect a more general regularity: the thermal destruction of the organic component intercalated into the MM interlayer space ultimately results in the formation of a graphene-like layer. In our case, the experimental evidences for such result follow from the analysis of Raman and IR spectra.

Figure 3 shows the Raman spectra for the PMM(xPVA) samples in the range from 1000 to 2000 cm^{-1}, which display a scattering band at ~1595 cm^{-1} (G-band), suggesting the presence of sp^2-carbon atom [10, 13, 14]. The intensity of this band is not high and increases with an increase in the PVA content in the starting composites. This result suggests the formation of relatively small in size graphene "islands," since continuous graphene layers in the interlayer space of MM give a high-intensity G-band [10].

Figure 4 shows, as an example, the IR spectra for the samples of Al_{13}-10PVA-MM and PMM(10PVA). One can assume that the graphene-like layers are cross-linked with the silicate ones due to silicon–carbon bonding in an unknown inversion of silicon–oxygen tetrahedra at elevated temperatures [15]. This is strongly confirmed by the relative increase in the intensity of peak arm corresponding to the apical Si–O vibrations in the silicon-oxygen tetrahedra (1100 cm^{-1}) compared to that of peak arm corresponding to the basal vibrations (1036 cm^{-1}) with increasing the calcination temperature [16]. In addition, the increase in the intensity of band at 800 cm^{-1} being typical of the Si–C bond is observed with an increase in temperature [17].

Thus, taking the abovementioned into consideration, the structural unit of the resulting layered columnar hybrid system is a pillar formed from the Keggin ion, which is cross-linked with the silicate layer on one side and with the graphene-like layer on the other side (Fig. 5). It is cross-linking with the latter which allows an explanation of the thermal stability of layered columnar structure: while the pillar is cross-linked with the silicate layer to form, most likely, only one Si_{layer}–O–Al_{pillar} bond, the cross-linking with the carbon layer can be provided through two or three $C_{graphene}$–O–Al_{pillar} bonds. In addition, when explaining high thermal stabilities of pillars, one can assume that processes related to the degradation features of the starting polymer during calcination of the samples are of importance. In particular, the radicals containing keto C=O groups form upon thermal destruction of PVA in the MM interlayer space [12]. Grafting of such radicals on the Al_{13} polycations can provide additional cross-links of pillars with the silicate and carbon layers due to the formation of oxygen bridges.

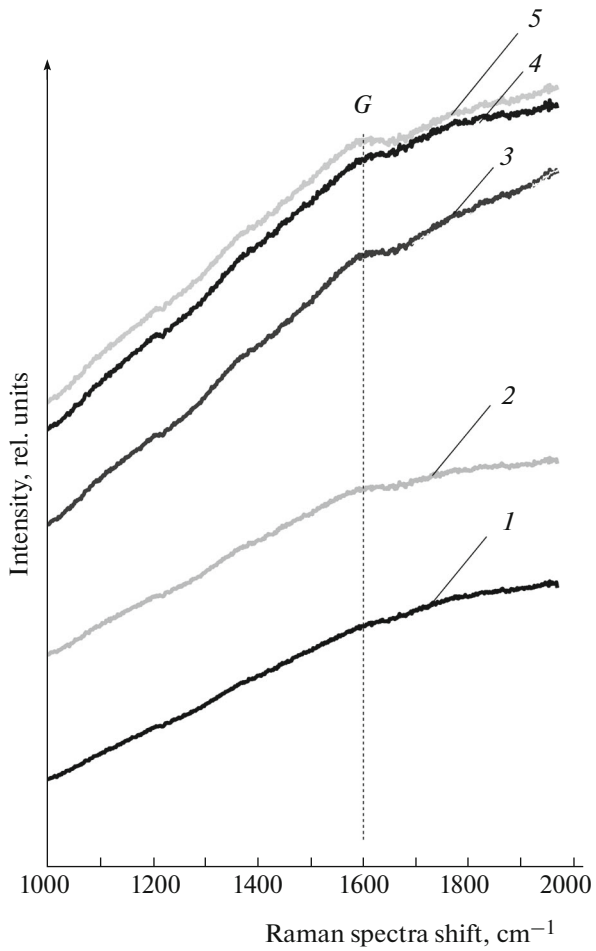

Fig. 3. Raman spectra of the PMM(*x*PVA) samples: (*1*) PMM(3PVA), (*2*) PMM(5PVA), (*3*) PMM(10PVA), (*4*) PMM(15PVA), and (*5*) PMM(20PVA).

The low-temperature nitrogen adsorption–desorption isotherms and pore-size distributions for the materials under study are given in Fig. 6. As can be seen from Fig. 6, the nitrogen adsorption isotherms for all samples relate to type IV according to the IUPAC classification [18] and are characterized by the presence of capillary condensation hysteresis loop, which is typical of materials having mesoporous structure. The shape of hysteresis loop in the relative pressure range from 0.4 to 0.9 relates to the type H3 [18] typical of porous materials with slit-shaped or plane-parallel pores.

For all samples, the amount of adsorbed N_2 is low under low relative pressure, but increases dramatically under high pressure close to $P/P_0 = 1$, which is caused by adsorption on macropores whose spaces are formed by the agglomeration of mesoporous particles [19]. The hysteresis loop of MM has a low area, which suggests the presence of mesopores between the parallel layers of material particles. The amount of nitrogen adsorbed on the intercalated Al_{13}-MM and pillar PMM samples is higher than that on the starting MM

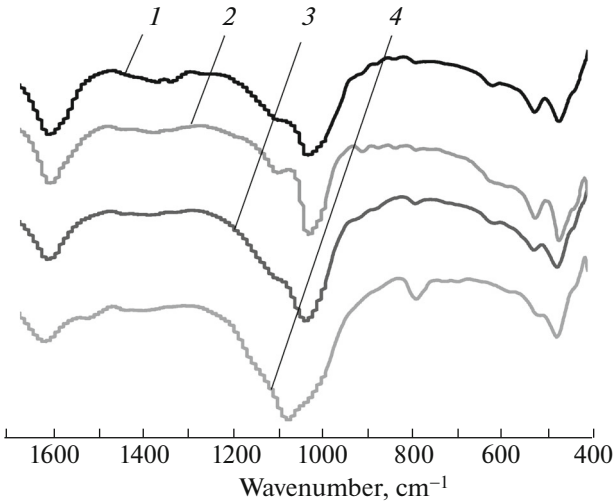

Fig. 4. IR spectra of the samples: (*1*) Al_{13}-10PVA-MM, (*2*) PMM(10PVA) (300°C), (*3*) PMM(10PVA) (450°C), and (*4*) PMM(10PVA) (600°C).

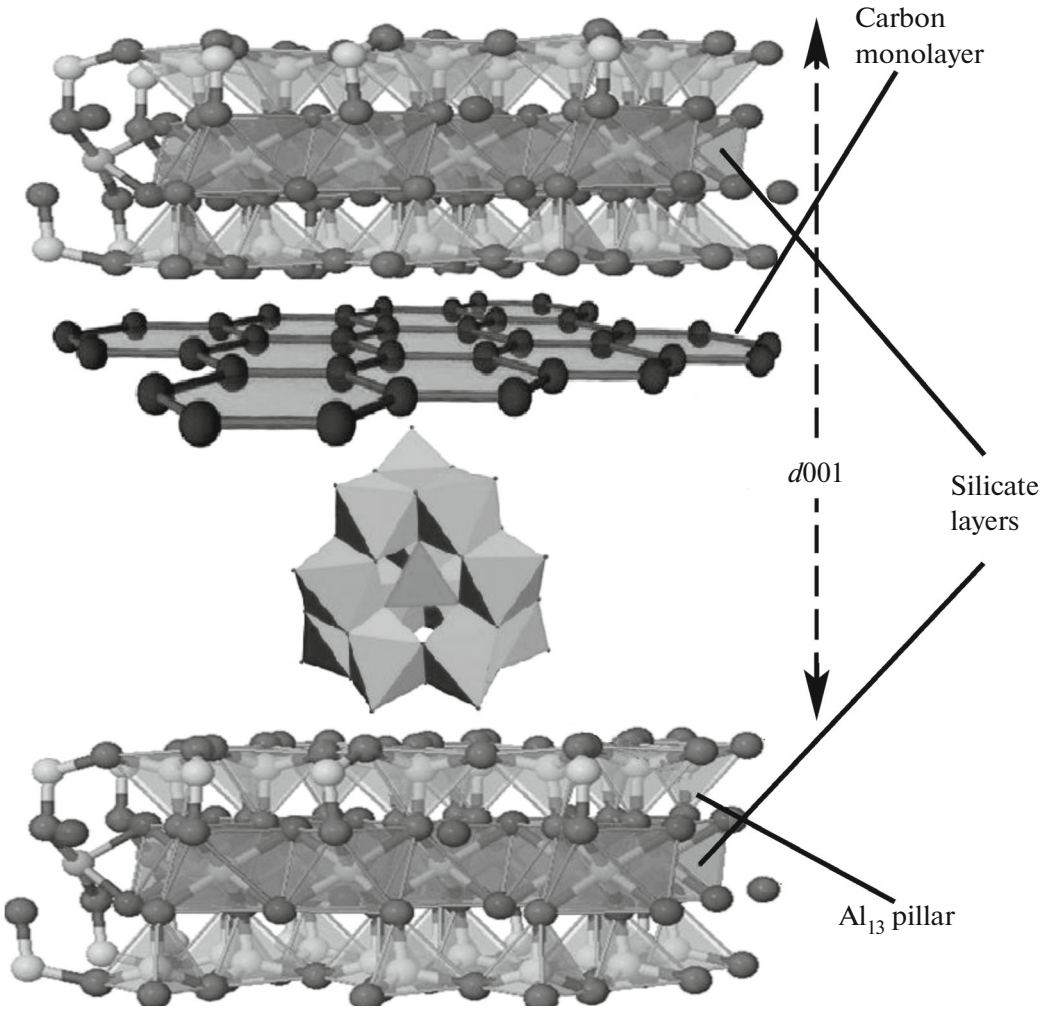

Fig. 5. Fragment of the hybrid layered columnar structure.

(Fig. 6a). This suggests that the intercalation of the Al_{13} polyhydroxocomplexes considerably improves the porous structure of montmorillonite.

The adsorption isotherms of pillar PMM(*x*PVA) samples (Figs. 6c, 6e, 6f) when compared to PMM (Fig. 6a) are characterized by a significant increase in the hysteresis loop area.

The values of specific BET surface area (S_{BET}), micropore volume (V_{mp}), mesopore volume (with a diameter from 1.7 to 300 nm) (V_{msp}), total pore volume ($\sum V_{pore}$), and average pore diameter (D_{av}) are given in Table 2. In general, the micropore volume of the PMM(*x*PVA) samples decreases compared to PMM. The specific surface area and total pore volume of the PMM(*x*PVA) samples calcinated at 300°C decreases when compared to the PMM sample. This is likely due to the fact the carbon formed upon degradation of PVA blocks pores. Annealing the samples at 450°C results in the partial burning of carbon, which, for samples with a PVA content of 10, 15, and 20 wt %, increases in the micropore volume, while the specific surface area and total pore volume are not different (excluding the PMM(10PVA) sample, having the maximum values of these parameters) from the samples calcinated at 300°C. The decrease in the S_{BET}, $\sum V_{pore}$, and V_{mp} values for the PMM(*x*PVA) ($x = 3$, 5, 10%) samples calcinated at 600°C is probably caused by the agglomeration of small pores into coarser ones, which is evidenced by the increase in the average pore diameter. Note that, on the samples calcinated at this maximum temperature, the specific surface area, total pore volume, and micro- and mesoporosities increase with an increase in the amount of PVA added. This result can be related to the burning of a higher amount of carbon formed in the samples between layers.

The pore-size distribution curves for all samples are shown in Figs. 6b, 6d, 6f, and 6h. All samples are characterized by a narrow unimodal pore-size distribution. The minimum average pore sizes of PMM(*x*PVA) correspond to PMM. The D_{av} values are

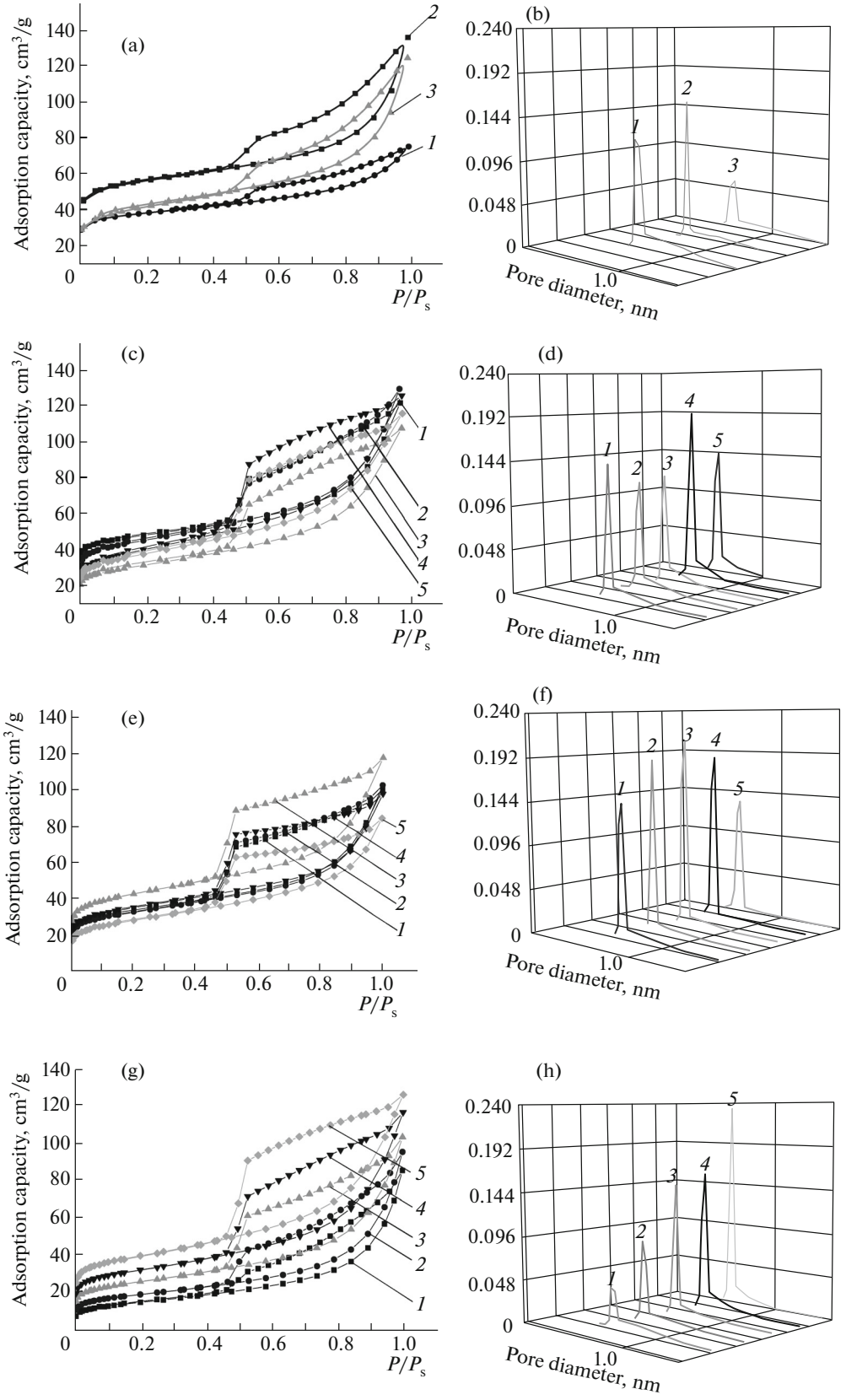

Fig. 6. Nitrogen adsorption–desorption isotherms and pore-size distributions for the samples of MM, Al_{13}-MM, and PMM (a, b): (*1*) MM, (*2*) Al_{13}-MM, (*3*) PMM, and those for PMM(*x*PVA) (c–h): (*1*) PMM(3PVA), (*2*) PMM(5PVA), (*3*) PMM(10PVA), (*4*) PMM(15PVA), and (*5*) PMM(20PVA).

within a wide enough range from 5.5 to 10.5 nm, depending on the parameter x and calcination temperature.

CONCLUSIONS

In this work, a new method for the formation of a carbon-containing layered columnar structure of montmorillonite by the intercalation of polyvinyl alcohol and aluminum polyhydroxocomplexes was proposed. On the one hand, PVA serves as an efficient delaminating agent at an intercalation step of Al_{13} ions. On the other hand, the degradation of the polymeric component at the step of pillar formation at elevated temperature creates conditions for (1) the formation of carbon layers with a graphene-like structure at the internal basal surfaces of the MM silicate layers and (2) grafting of the radical degradation products on the Al_{13} polycations followed by the cross-linking of pillars with carbon and silicate layers. The most important result is that the thermally stable layered columnar system undergoes no collapse even at 600°C, in contrast to the widely used Al_2O_3-pillar MM, which demonstrates structural stability only up to 400°C. The textural characteristics of the carbon-containing pillar samples are found to be at the same level. Moreover, they can be varied within certain limits according to the amount of polymer added and calcination temperature.

Taking into account that the increase in the thermal stabilities of pillar materials is one of the key points in their successful engineering application on an industrial scale, the procedure for the formation of layered columnar systems using polymeric additives can be used in the preparation of selective absorbents, molecular sieves, and catalyst supports.

ACKNOWLEDGMENTS

This work was financially supported by the Russian Foundation for Basic Research (Grant No. 13-03-00673).

REFERENCES

1. F. M. Fernandes, H. Baradari, and C. Sanchez, Appl. Clay Sci. **100**, 2 (2014).
2. M. A. Vicente, A. Gil, and F. Bergaya, "Pillared clays and clay minerals," in *Handbook of Clay Science,* 2nd Ed. (Elsevier, Amsterdam, 2013), Vol. 5A, p. 524.
3. M. F. Butman, N. L. Ovchinnikov, V. V. Arbuznikov, and A. V. Agafonov, Izv. Vyssh. Uchebn. Zaved., Khim. Khim. Tekhnol. **55** (8), 73 (2012).
4. A. G. Belozerov, N. S. Karasev, N. L. Ovchinnikov, and M. F. Butman, Nanotech. Russ. **9** (7–8), 410 (2014).
5. Y. Gao, W. Li, H. Sun, Z. Zheng, X. Cui, H. Wang, and F. Meng, Appl. Clay Sci. **88–89**, 228 (2014).
6. Z. Qin, P. Yuan, S. Yang, D. Liu, H. He, and J. Zhu, Appl. Clay Sci. **99**, 229 (2014).
7. V. V. Nasedkin, *Dash-Sakhalin Precast Concrete Deposition (Establishing and Development Trends)* (GEOS, Moscow, 2008), p. 85 [in Russian].
8. M. F. Butman, N. L. Ovchinnikov, V. V. Arbuznikov, A. V. Agafonov, and B. Nuralyev, Pis'ma Mater. **3** (4), 284 (2013).
9. A. Gil, S. A. Korili, and M. A. Vicente, Cat. Rev.-Sci. Eng. **50** (2), 153 (2008).
10. Q. Chen, R. Zhu, W. Deng, Y. Xu, J. Zhu, Q. Tao, and H. He, Appl. Clay Sci. **100**, 112 (2014).
11. O. Albreksten, R. L. Eriksen, S. M. Novikov, D. Schall, M. Karl, S. I. Bozhevolnyi, and A. C. Simonsen, J. Appl. Phys. **111**, 305 (2012).
12. U. H. Hossain, T. Seidl, and W. Ensinger, Polym. Chem. **5**, 1001 (2014).
13. C. Tikhomirov and T. Kimstach, Analitika, No. **1**, 28 (2011).
14. E. Ruiz-Hitzky, M. Darder, F. M. Fernandes, E. Zatile, F. J. Palomares, and P. Aranda, Adv. Mater. **23**, 5250 (2011).
15. H. Slosiarikova, J. Bujdak, and V. Hlavaty, J. Incl. Phenom. Molec. Recogn. Chem. **13**, 267 (1992).
16. X. Hongyan and C. Xingtong, Adv. Mat. Res. **187**, 112 (2011).
17. K. L. Vyshniakova, L. N. Pereselentseva, V. P. Red'ko, and T. V. Tomila, Composit. Nanostruct., No. 2, 28 (2010).
18. K. S. W. Sing, D. H. Everett, R. A. W. Haul, et al., Pure Appl. Chem. **57** (4), 603 (1985).
19. M. Xia, Y. Jiang, L. Zhao, F. Li, B. Xue, M. Sun, D. Liu, and X. Zhang, Colloids Surf. A **356**, 1 (2010).

Translated by K. Utegenov